Point-defect optical transitions and thermal ionization energies from quantum Monte Carlo methods: Application to the *F*-center defect in MgO

Elif Ertekin,* Lucas K. Wagner,† and Jeffrey C. Grossman‡

Department of Materials Science and Engineering, Massachusetts Institute of Technology, Cambridge, Massachusetts 02139, USA

(Received 2 October 2012; published 30 April 2013)

We present an approach to calculation of point-defect optical and thermal ionization energies based on the highly accurate quantum Monte Carlo methods. The use of an inherently many-body theory that directly treats electron correlation offers many improvements over the typically employed density functional theory Kohn-Sham description. In particular, the use of quantum Monte Carlo methods can help overcome the band-gap problem and obviate the need for *ad hoc* corrections. We demonstrate our approach to the calculation of the optical and thermal ionization energies of the *F*-center defect in magnesium oxide, and obtain excellent agreement with experimental and/or other high-accuracy computational results.

DOI: 10.1103/PhysRevB.87.155210 PACS number(s): 71.15.Qe, 71.20.Nr, 71.55.Gs, 78.55.Et

I. INTRODUCTION

From electronics to optoelectronics to photovoltaics, point defects influence and often dominate the properties of semiconducting materials.[1–6] Quantitative descriptions of the effect of point defects on electronic, optical, and transport properties is critical to enabling point-defect engineering for materials design. However, accurate prediction of point-defect energetics, thermal ionization energies, and optical transition energies from first principles remains a challenge. Currently, the most widely used approach based on conventional density functional theory (DFT) suffers from poor descriptions of band gaps, which render difficult the accurate description of midgap defect states.[5,7–9] Here we demonstrate that, by contrast, an inherently many-body approach based on quantum Monte Carlo (QMC) methods[10,11] can eliminate these problems and enable high-accuracy calculations of point-defect optical and thermal ionization energies. Our computed optical transition energies are in excellent agreement with experimental and other high-accuracy computational results for the same system,[12] and demonstrate that QMC can obtain quantitatively accurate descriptions.

QMC methods comprise a suite of stochastic tools that enable calculations of material properties based on the many-particle Schrödinger equation. Because of their direct treatment of electron correlation, QMC methods are among the most accurate electronic structure approaches available today, and demonstrate a long and distinguished record of groundbreaking and benchmarking calculations.[10,11,13] In comparison to the other "beyond-DFT" techniques that are currently explored for calculation of point-defect properties (DFT + U, hybrid DFT, and the GW method), QMC is directly based on the true many-body Schrödinger equation and offers the possibility of parameter-free accurate band gaps and total energies. The application of QMC techniques to point defects in solids is still a relatively new field. To date, a handful of studies have been carried out to compute defect formation energies: interstitials in silicon,[14–16] vacancies in diamond,[15] the Schottky defect in MgO,[17] and vacancies and interstitials in aluminum.[18]

In this contribution, we illustrate the application of the QMC method to the *F*-center defect (oxygen vacancy) in magnesium oxide (MgO) by computing defect formation energies, thermal ionization levels, and optical ionization energies (although the approach is general and can be extended to other materials of interest). The *F*-center defect in MgO is a typical example of an intrinsic point defect in a binary ionic compound.[19–24] Despite its apparent simplicity, its properties as deduced from optical absorption and luminescence studies have proven somewhat ambiguous. Experimental characterization of the *F* center in its neutral (F^0) and singly ionized (F^{+1}) state has been complicated by their nearly identical optical absorption energies.[22–24] These energies have been corroborated by recent GW calculations;[12] which also predicted optical emission energies that are substantially different from the assigned experimental values, causing the authors to suggest a reinvestigation of the experimental observations. A particularly compelling possibility is to explore the *F*-center defect using distinct high-accuracy first-principles techniques to compare results. Our results—calculated independently using QMC methods—corroborate the GW results and further invite reassessment of the experimental data for the optical emission energies.

II. METHODOLOGY AND BENCHMARKING

A. Density functional theory

We first compute the properties of the *F*-center defect in MgO within a DFT[25,26] framework as implemented in the SIESTA code,[27] employing the Perdew-Burke-Ernzerhof[28] approximation to the exchange correlation potential. The inner core electrons are represented by Troullier-Martins pseudopotentials (leaving the Mg 3*s* and O 2*s*, 2*p* electrons in valence), and the Kohn-Sham orbitals are represented by a linear combination of numerical pseudoatomic orbitals expanded in a triple ζ with polarization basis set. For bulk rocksalt MgO, in agreement with previous DFT calculations[29,30] we find a lattice parameter of 4.25 Å (4.22 Å in experiment[31]), an atomization energy of 9.50 eV/MgO (10.50 eV/MgO in experiment[31]), and a direct band gap of 4.83 eV at the Γ point (a considerable underestimate of the experimental band gap of 7.78 eV[32]).

The DFT band-gap underestimate has a severe consequence on the prediction of midgap defect states, defect energetics (particularly for occupied defect levels), and defect-induced optical absorption and emission energies. Broadly, the

TABLE I. Comparison of bond length, binding energy, and electron affinity for the MgO molecule according to DMC and in experiment. Two sets of DMC results are provided, corresponding to the use of neon-core (large) and helium-core (small) pseudopotentials. Error bars are shown in parentheses.

	bond length (Å)	binding energy (eV)	electron affinity (eV)
DMC, Ne-core PP	1.75	2.28(1)	1.76(1)
DMC, Ar-core PP	1.75	2.43(1)	1.72(1)
Exp. (Refs. 31,33–35)	1.75	2.56(21)	1.630(25)

band-gap underestimate arises because in typically employed mappings of the interacting many-body Schrödinger equation to the DFT single-particle effective-potential Kohn-Sham equations, each electron also interacts with itself (self-interaction error[37–41]). This results in an extraneous Coulomb repulsion that overly delocalizes electronic states. The self-interaction error, in addition to the absence of a derivative discontinuity in the exchange-correlation potential,[37–41] results in underestimated band gaps that have plagued DFT calculations.

B. Quantum Monte Carlo

The QMC calculations reported here are computed within fixed-node diffusion Monte Carlo (FN-DMC) as implemented in the QWALK code,[42] with single-determinant Slater-Jastrow trial wave functions constructed from the DFT orbitals, variance-minimized Jastrow coefficients, and a time step of 0.01 au. To establish that our choice of pseudopotentials is reasonable, we first calculated the bond length, electron affinity, and binding energy of the MgO molecule within DMC.

We tested both Ne- and He-core pseudopotentials for the Mg atom in the molecule, and found that (although both give good results) the small core pseudopotential gives a somewhat better description as shown in Table I. While both pseudopotentials give excellent agreement to the experimental bond length and electron affinity, we find some difference for the binding energy and the ionization energy. Using a He-core, rather than Ne-core, pseudopotential for Mg increases the molecular binding energy from 2.28 ± 0.01 eV to 2.43 ± 0.01 eV, in comparison to the experimental value of 2.54 ± 0.22 eV.[31,33–35] This suggests that allowing the Mg $2s$ and $2p$ electrons to participate in the bonding recovers more of the binding energy. We also find that using the Ne-core pseudopotential introduces a small 0.04(2) eV error in the ionization energy compared to the He-core pseudopotential. These observations suggest that including the Mg $2s$ and $2p$ electrons improves the description slightly; however, for the solid, the computational cost of the He-core pseudopotential was too prohibitive.

Next, to test the properties of the defect-free MgO solid in QMC, we calculate the following states: the ground state E_o, the Γ-point optically excited state $E_{\Gamma\to\Gamma}$, the positively charged state E_+, and the negatively charged state E_-. From the ground-state energy E_o, we compute the atomization energy of the MgO solid using twist-averaged boundary conditions and the extrapolation framework described in Refs 43–45 with supercells containing 16, 32, and 64 atoms as shown in Fig. 1. The dependence of the binding energy on the supercell size reflects the spurious electron correlation that appears in many-body theories when periodic boundary conditions are applied. This spurious correlation disappears in the infinite-size supercell limit. The extrapolated value of the atomization energy in DMC is 10.18 ± 0.05 eV per formula unit, in comparison to the experimental and DFT values of 10.5 eV and 9.48 eV, respectively.[31,32,36] Although DMC improves the atomization energy in comparison to DFT, it is most likely necessary to include the Mg $2s$ and $2p$ electrons in valence to obtain atomization energies closer to experiment.

The ionization potential (IP), electron affinity (EA), quasiparticle gap (QP), and optical gap (OP) are given by

$$\mathrm{IP} = E_o - E_+ \tag{1}$$

$$\mathrm{EA} = E_- - E_o \tag{2}$$

$$\mathrm{QP} = \mathrm{EA} - \mathrm{IP} \tag{3}$$

$$\mathrm{OP} = E_{\Gamma\to\Gamma} - E_o \tag{4}$$

and are similarly computed by extrapolation, as illustrated in Fig. 2. Here we use only the Γ-point orbitals to construct the many-particle wave function, to reduce computational cost and since the MgO solid exhibits a direct band gap at the Γ point. For these quantities, additional finite-size effects are present including (i) periodic image interactions between the electron-hole pair for the optical gap and (ii) the electrostatic interaction between charged supercells in the calculation of the ionization potential and electron affinity. Extrapolating to the infinite supercell limit, we obtain an optical gap of 7.96 ± 0.06 eV and a quasiparticle gap of 7.89 ± 0.10 eV, in close agreement with the experimental band gap of 7.8 eV.

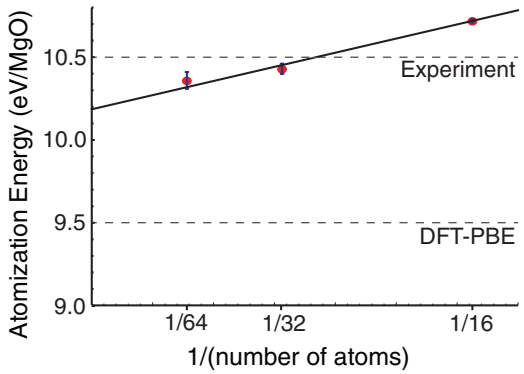

FIG. 1. (Color online) The extrapolated value of the atomization energy as computed in DMC is 10.18 ± 0.05 eV, in comparison to the experimental and DFT values of 10.5 eV and 9.48 eV, respectively (Refs. 31, 32, and 36).

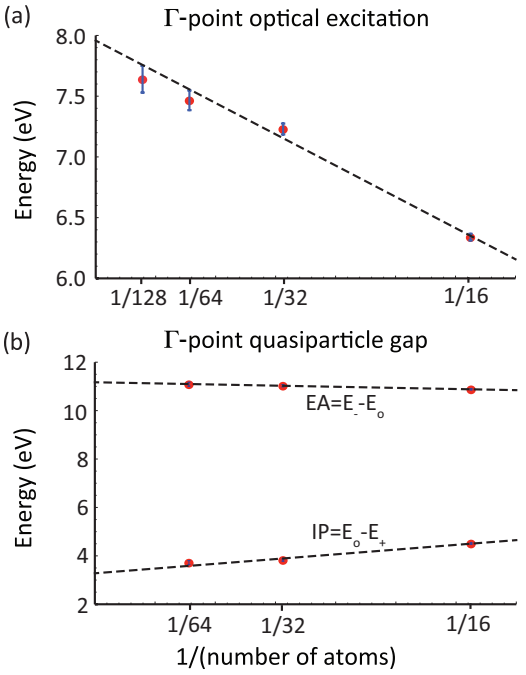

FIG. 2. (Color online) Optical and quasiparticle gap in MgO obtained by extrapolating supercells to infinite size. The data points for finite-size supercells are computed with DMC. The extrapolated value of the optical gap is 7.96 ± 0.06 eV. The extrapolated ionization potential $\mathrm{IP} = E_o - E_+ = 3.28 \pm 0.07$ eV. The extrapolated electron affinity $\mathrm{EA} = E_- - E_o = 11.17 \pm 0.07$ eV. This gives a quasiparticle gap of $\mathrm{QP} = \mathrm{EA} - \mathrm{IP} = 7.89 \pm 0.10$ eV. [Note the EA and IP are referenced to the average electrostatic potential in the supercell.]

The results are summarized in Table II, and show excellent agreement overall with the experimental values. The slight underestimation of the atomization energy is likely due to the Ne-core pseudopotential, since the MgO molecule showed a similar effect, while the gap calculations are close to experiment, overestimating the gap slightly.

III. DEFECT CALCULATIONS

For the F-center defect, we use 64 (perfect) and 63 (with F-center) atom supercells for these calculations. In Fig. 3, we show the DFT-computed electronic band structure of a 63-atom MgO supercell containing an F^0-center defect (neutral oxygen vacancy). In agreement with previous DFT calculations,[12] the F^0-center introduces a fully occupied midgap defect level of a_{1g} symmetry into the electronic band structure; higher in the conduction band we also find a triply degenerate excited defect level of t_{1u} symmetry.

TABLE II. Comparison of lattice constant, atomization energy, and band gap in MgO solid according to DFT, DMC, and in experiment. All computed results are obtained using Ne-core pseudopotentials for magnesium. The optical band gap is determined in DFT from the Kohn-Sham levels, and in DMC from the extrapolated optical excitation energy. Error bars are shown in parentheses. Note that the IP and EA are given with respect to the average potential in the supercell.

	DFT-PBE	DMC	Exp (Refs. 31, 32, and 36)
Lattice const (Å)	4.25	4.22	4.216
Coh. En. (eV/MgO)	9.50	10.18(5)	10.5
OP (eV)	4.83	7.96(6)	7.78
QP (eV)	–	7.9(1)	7.84
IP (eV)	–	3.28(7)	–
EA (eV)	–	11.17(7)	–

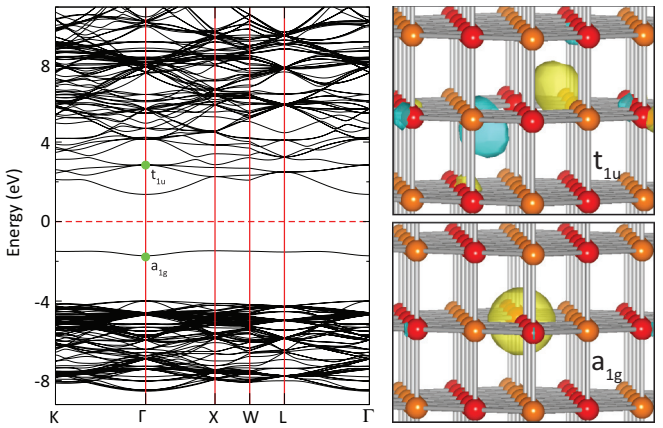

FIG. 3. (Color online) Left: The electronic band structure of a 64-atom MgO supercell containing a single oxygen vacancy, calculated within DFT-PBE. The neutral oxygen vacancy introduces a localized midgap defect level of symmetry a_{1g}. There is also a triply degenerate excited defect level in the conduction band of t_{1u} symmetry. Right: The corresponding a_{1g} and t_{1u} Kohn-Sham states plotted at the Γ point, showing the localized nature in the vicinity of the vacancy.

We obtain defect formation energies $\Delta E_{D,q}$ according to

$$\Delta E_{D,q} = (E_{D,q} - E_{\mathrm{perf}}) - \sum_i n_i \mu_i + q(E_V + E_F), \quad (5)$$

where $E_{D,q}$ is the (computed) total energy of the supercell containing a defect D in the charge state q, E_{perf} is the (computed) total energy of the perfect supercell, and n_i is the number of atoms of species i added to ($n_i > 0$) or removed from ($n_i < 0$) the supercell to create the defect.[46] Different environmental conditions are accommodated by the set of chemical potentials μ_i for each element by assuming that each is in equilibrium with a physical reservoir such as a gas or a bulk phase. E_V is the energy of the valence band maximum (the ionization potential in DMC), and E_F is the Fermi energy referenced to E_V so that $0 \leqslant E_F \leqslant E_g$ where E_g is the band gap.

A. Thermal ionization levels

The thermal ionization energies, which determine the shallow or deep nature of a defect, correspond to the Fermi energies at which the energetically most-favored charge state of the defect changes. According to our DFT calculations, the creation of an F^0 center results in the formation of a filled midgap defect level (shown in Fig. 3). There is very little lattice relaxation that takes place upon removal of the O, as indicated in Table III. However, when an electron is removed from the supercell to form the F^{+1} center, in DFT we find a large lattice relaxation as the positively charged Mg ions move outward away from, and the negatively charged O ions move inward toward, the positively charged vacancy in conjunction

TABLE III. DFT-computed lattice relaxations for the F, F^{+}, and F^{+2} center. The Mg-Mg distance denotes the separation between Mg atoms that neighbor the missing O atom; similarly the O-O distance denotes the separation between O atoms that neighbor the missing O atom.

	Mg-Mg (Å)	O-O (Å)	Relaxation (eV)
perfect	2.98	5.96	–
F	2.99	5.96	0.003
F^{+}	3.09	5.90	0.545
F^{+2}	3.17	5.84	1.182

with a 0.55 eV drop in energy. Further ionizing the defect to the F^{+2} state in DFT results in further lattice relaxations accompanied by an energy recovery of 1.18 eV. The DFT defect formation energies obtained from Eq. (5) are plotted in Fig. 4(a), showing thermal ionization levels near the middle of the gap (plotted here for the Mg-rich limit). In Fig. 4(a), we have used the as-computed DFT band gap for MgO, without correction schemes to artificially open the gap.

For the F^{+1} and F^{+2} defect, the nonzero net charge in the simulation cell introduces electrostatic image interactions between neighboring supercells. For the charged supercells, the screened interaction energy of the periodically arranged

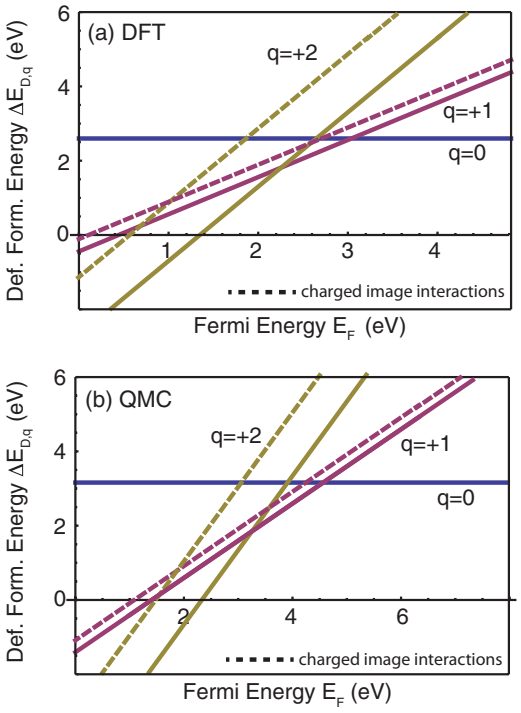

FIG. 4. (Color online) Comparison of F-center defect formation energies and thermal ionization energies in MgO computed in DFT and DMC. The domain of the Fermi energy (x axis) is determined by the band gap of the system according to the computational framework; clearly the DMC description of the gap is better and obviates the need for band-gap corrections. In comparison to DFT, DMC modifies somewhat the absolute value of the defect formation energies, but maintains thermal ionization levels near midgap. [Note that the error bars of the DMC-computed formation energies are smaller than the line widths in (b).]

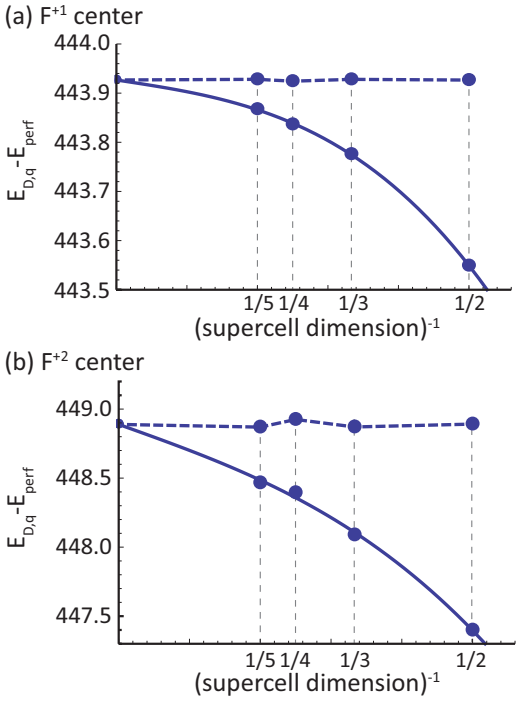

FIG. 5. (Color online) Charge extrapolation computed within DFT.

charged defect and the compensating background is estimated within DFT via an extrapolation approach.[47] Figure 5 illustrates the extrapolation for the singly and doubly charged oxygen vacancy for supercells of size $n \times n \times n, n = 2,3,4,5$. The solid curved line shows the fit

$$E_T\left(\frac{1}{L}\right) = E_T\left(\frac{1}{L} \to 0\right) - \frac{A}{L} - \frac{B}{L^3}, \tag{6}$$

in which L^3 denotes the volume of the supercell and A, B are the fitting parameters. The dashed lines in Fig. 5 show the total energy for each supercell when the finite-size error is estimated by Eq. (6). Based on the extrapolated value of the total energy in the dilute limit, the charged defect interactions introduce a finite-size error of 0.38 eV and 1.49 eV for the F^{+1} and F^{+2} centers, respectively, for the $2 \times 2 \times 2$ supercells that we use in our analysis. The dotted lines shown in Fig. 4(a) show the defect formation energies for the F^{+1} and F^{+2} centers, now incorporating this estimate of the charged image interaction energy.

For the QMC calculations of total energies of perfect and defect supercells (E_{perf}, $E_{D,q}$) and the corresponding thermal ionization levels, we use the relaxed lattice geometries of and orbitals obtained from the DFT calculations. Total supercell energies are again obtained using twist-averaged boundary conditions. Figure 4(b) shows the defect formation energies and the thermal ionization levels as computed within QMC. Again, the solid lines indicate the formation energies obtained when charged image interactions are ignored, and the dotted lines indicate the shift that occurs when the *DFT estimate* of the charged image interactions is incorporated. We have not carried out the extrapolation within DMC: while this can be done in principle, it remains prohibitively expensive from a computational standpoint. However, we note that this would be of interest, as it is very likely that the DFT and QMC estimate

of charged image interactions will be different, owing to the difference in electron localization and thus screening for the two approaches.

To compare the DFT- and the QMC-obtained defect formation energies in Fig. 4, we note first that for the F-center defect, both DFT and QMC put the defect thermal ionization energies near midgap. This qualitative similarity is not expected to hold for all material systems (especially for wide-gap semiconductors or correlated systems for which the DFT gap error is more insidious). In our case, MgO is an ionic solid according to both DFT and QMC (albeit less so with the former), and both approaches give qualitatively similar behavior. The largest single difference between the DFT and the QMC results is, of course, the domain for the Fermi energy $0 < E_F < E_g$. From Fig. 4, the overall formation energy of the neutral defect (F^0) is higher in QMC by approximately 0.5 eV. This increase in formation energy may be largely attributed to the fact that while QMC captures the highly localized, ionic nature of the solid, DFT-PBE renders the MgO system slightly more delocalized than in reality.

We can investigate the localization of the two approaches by calculating the site-resolved charge fluctuations, also known as the compressibility of a site (Fig. 6). We evaluate the expectation value $\langle\Psi|(\hat{n}_i - \langle\hat{n}_i\rangle)^2|\Psi\rangle$, where the $\hat{n}_i$ is number operator on the Voronoi polyhedron surrounding atomic site i. If this quantity is larger, then the system is more metal-like with mobile charges, and if it is smaller, then the system is more insulating with larger barriers to charge movement. In Fig. 6, one can see that the DFT charge fluctuations of the Mg atoms near the defect track the QMC values surprisingly well. The main difference between the two theories is that the oxygen charge fluctuations are much larger in DFT, which is related to the underestimation of the gap. We thus conclude that the main error of DFT in the case of the F-center defect in MgO is excess delocalization in the oxygen bands.

The overly delocalized (more metal-like, with a smaller band gap) description in DFT makes the penalty for bond breaking too small, and consequently the defect formation energy too small as well. The effect on computed defect energies are significant for defects with occupied midgap defect levels such as the F^0 center. As a result of the underestimated band gap, in DFT the Kohn-Sham level of the deep, doubly occupied F^0 level is squeezed too close to the valence band maximum, directly resulting in a low calculated formation energy. Our finding here is similar to the findings for the formation energies of neutral, interstitial Si atoms in silicon,[14–16] for which DMC calculations show that DFT underestimates formation energies in the case of occupied midgap defect levels. This analysis is also consistent with recent QMC results for defect formation energies in aluminum:[18] for metallic systems, for which DFT delocalization problems are less significant, the DMC results are more closely matched.

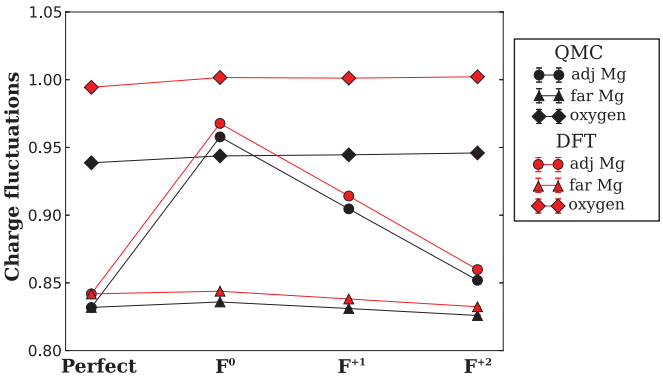

FIG. 6. (Color online) The charge fluctuations $\langle\Psi|(\hat{n}_i - \langle\hat{n}_i\rangle)^2|\Psi\rangle$ for a Slater determinant of DFT (PBE) Kohn-Sham orbitals (red, upper curves) and QMC (FN-DMC) wave function (black, lower curves), for the perfect MgO 64 atom cell, and the defective 63-atom cell in different charge states. The fluctuations are site resolved into the Mg atoms adjacent to the F-center defect (circles), Mg atoms further away from the defect (triangles), and oxygen atoms (diamonds). Stochastic uncertainties are smaller than the symbol size.

B. Optical transitions: absorption and emission

We now turn to the QMC description of the optical ionization energies, corresponding to vertical Franck-Condon transitions on a configuration coordinate diagram as illustrated in Fig. 7. An optical transition occurs when a photon is absorbed or emitted by the defect; because this transition takes place essentially instantaneously on the scale of lattice relaxations it occurs at fixed atomic coordinates (and hence is represented as a vertical transition). Such a transition places the system in an excited vibrational state; for example, F^0-center absorption illustrated in Fig. 7 refers to the absorption of a photon and the promotion of an electron from the filled midgap level to the conduction band, leaving behind an electron in the conduction band and an F^{+1} center in an excited vibrational state (which soon decays to the F^{+1} vibrational ground state). Therefore, we compute the optical transitions by using the relaxed coordinates of the initial state, and occupying the

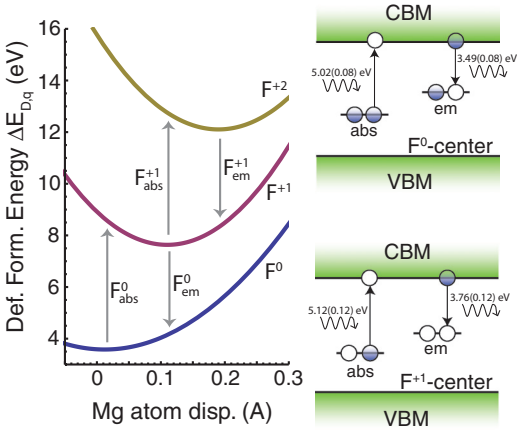

	F^0_{abs}	F^0_{em}	F^{+1}_{abs}	F^{+1}_{em}
QMC	5.0(1)	3.8(1)	5.1(1)	3.5(1)
GW[8]	4.95	3.6	4.92	3.4
Exp	5.00	3.1-3.2	4.95	2.3-2.4

FIG. 7. (Color online) Optical absorption and emission energies (in eV) computed in DMC for the F-center defect in MgO. The DMC absorption energies are in excellent agreement with experiment and recently published GW results. The DMC emission energies are in disagreement with the experimentally assigned values, but match closely to the GW results.

Kohn-Sham orbitals as appropriate to describe the vibronic state. Although we do not include charged supercell interactions here, we note that their effect should be smaller here than in the case of the thermal ionization energies above, since now we are comparing energies of supercells with the same net charge.

Our DMC absorption energies (Fig. 7) are in excellent agreement with experiment and remarkably close to the GW-computed values, demonstrating the high-accuracy potential of the DMC methodology. The DMC emission energies are also remarkably similar to the GW-computed values, but in disagreement with the experimental numbers. The disagreement between the GW and experimental values led the authors in Ref. 8 to suggest that the low energy signal around 2.3–2.4 eV that is observed in fact arises when electrons in the defect level recombine with holes in the valence band. We find it notable that two distinct many-body approaches (namely QMC and GW) have yielded similar results for the optical emission transitions in question.

This leads us to suggest two possibilities. First, we find it likely that, as suggested by the authors in Ref. 8, the original emission-peak assignment should be revisited. A second possibility is based on the fact that both our QMC and the GW results are built from DFT-relaxed atomic geometries (Table III). It is possible that the GW and QMC results compare favorably because both methods are using similar DFT-relaxed lattice geometries. If the relaxations are not properly described in DFT, then the many-body energies may be similar but incorrect. However, the possibility that the lattice geometries are problematic seems unlikely given the exceptional agreement with experiment for the absorption transitions.

IV. CONCLUSION

In conclusion, we demonstrate the application of quantum Monte Carlo methods to the calculation of the thermal and optical ionization energies of point defects in solids. The striking agreement between two highly accurate methods, quantum Monte Carlo and GW, suggests that predictive calculations of point-defect properties are now in reach. Due to its inherently many-body approach and accurate treatment of electron correlation, quantum Monte Carlo shows large promise for the quantitative first-principles calculation of point-defect properties.

ACKNOWLEDGMENTS

We gratefully acknowledge fruitful discussions with S. B. Zhang, Y. Y. Sun, P. Zhang, and T. Abtew. This work was supported by DOE Grant No. DE-SC0002623. Calculations were performed in part at the National Energy Research Scientific Computing Center of the Lawrence Berkeley National Laboratory and in part by the National Science Foundation through TeraGrid resources provided by NCSA under Grant No. TG-DMR090027 and Grant No. TG-DMR120080, and through the Blue Waters Early Science program.

*Present address: University of Illinois; ertekin@illinois.edu
†Present address: University of Illinois; lkwagner@illinois.edu
‡jcg@mit.edu

[1] D. J. Chadi and K. J. Chang, Phys. Rev. Lett. **61**, 873 (1988).
[2] S. B. Zhang and D. J. Chadi, Phys. Rev. B **42**, 7174 (1990).
[3] C. G. Van de Walle, P. J. H. Denteneer, Y. Bar-Yam, and S. T. Pantelides, Phys. Rev. B **39**, 10791 (1989).
[4] S. B. Zhang, S.-H. Wei, A. Zunger, and H. Katayama-Yoshida, Phys. Rev. B **57**, 9642 (1998).
[5] C. G. Van de Walle and J. Neugebauer, J. Appl. Phys. **95**, 3851 (2004).
[6] C. H. Park, S. B. Zhang, and S.-H. Wei, Phys. Rev. B **66**, 073202 (2002).
[7] S. Lany and A. Zunger, Phys. Rev. B **78**, 235104 (2008).
[8] P. Rinke, A. Janotti, M. Scheffler, and C. G. Van de Walle, Phys. Rev. Lett. **102**, 026402 (2009).
[9] D. A. Drabold and S. Estreicher, in *Topics in Applied Physics* (Springer-Verlag, Berlin, 2007), pp. 11–27.
[10] F. R. Petruzielo, J. Toulouse, and C. J. Umrigar, J. Chem. Phys. **136**, 124116 (2012).
[11] W. M. C. Foulkes, L. Mitas, R. J. Needs, and G. Rajagopal, Rev. Mod. Phys. **73**, 33 (2001).
[12] P. Rinke, A. Schleife, E. Kioupakis, A. Janotti, C. Rödl, F. Bechstedt, M. Scheffler, and C. G. Van de Walle, Phys. Rev. Lett. **108**, 126404 (2012).
[13] J. C. Grossman, J. Chem. Phys. **117**, 1434 (2001).
[14] E. R. Batista, J. Heyd, R. G. Hennig, B. P. Uberuaga, R. L. Martin, G. E. Scuseria, C. J. Umrigar, and J. W. Wilkins, Phys. Rev. B **74**, 121102(R) (2006).
[15] R. Q. Hood, P. R. C. Kent, R. J. Needs, and P. R. Briddon, Phys. Rev. Lett. **91**, 076403 (2003).
[16] W. D. Parker, J. W. Wilkins, and R. G. Hennig, Phys. Status Solidi B **248**, 267 (2010).
[17] D. Alfè and M. J. Gillan, Phys. Rev. B **71**, 220101(R) (2005).
[18] R. Q. Hood, P. R. C. Kent, and F. A. Reboredo, Phys. Rev. B **85**, 134109 (2012).
[19] B. T. Jeffries, R. Gonzalez, Y. Chen, and G. P. Summers, Phys. Rev. B **25**, 2077 (1982).
[20] G. H. Rosenblatt, M. W. Rowe, G. P. J. Williams, R. T. Williams, and Y. Chen, Phys. Rev. B **39**, 10309 (1989).
[21] Y. Chen, J. L. Kolopus, and W. A. Sibley, Phys. Rev. **186**, 865 (1969).
[22] L. A. Kappers, R. L. Kroes, and E. B. Hensley, Phys. Rev. B **1**, 4151 (1970).
[23] J. Kemp, J. Cheng, E. Izen, and F. Modine, Phys. Rev. **179**, 818 (1969).
[24] Y. Chen, V. M. Orera, R. Gonzalez, R. T. Williams, G. P. Williams, G. H. Rosenblatt, and G. J. Pogatshnik, Phys. Rev. B **42**, 1410 (1990).
[25] P. Hohenberg and W. Kohn, Phys. Rev. **136**, 864 (1964).
[26] W. Kohn and L. J. Sham, Phys. Rev. **140**, 1133 (1965).
[27] E. Artacho, E. Anglada, O. Diéguez, J. D. Gale, A. García, J. Junquera, R. M. Martin, P. Ordejón, J. M. Pruneda, D. Sánchez-Portal, and J. M. Soler, J. Phys.: Condens. Matter **20**, 064208 (2008).
[28] J. P. Perdew, K. Burke, and M. Ernzerhof, Phys. Rev. Lett. **77**, 3865 (1996).

[29]F. Marinelli and A. Lichanot, Chem. Phys. Lett. **367**, 430 (2003).
[30]A. Schleife, F. Fuchs, J. Furthmüller, and F. Bechstedt, Phys. Rev. B **73**, 245212 (2006).
[31]NIST chemistry webbook, online: http://webbook.nist.gov.
[32]R. C. Whited and W. C. Walker, Phys. Rev. Lett. **22**, 1428 (1969).
[33]L. Operti, E. C. Tews, T. J. MacMahon, and B. S. Freiser, J. Am. Chem. Soc. **111**, 9152 (1989).
[34]J. H. Kim, X. Li, L.-S. Wang, H. L. de Clercq, C. A. Fancher, O. C. Thomas, and K. H. Bowen, J. Phys. Chem. A **105**, 5709 (2001).
[35]J. M. Recio, A. Ayuela, R. Pandey, and A. B. Kunz, Z. Phys. D Supplement **26**, 273 (1993).
[36]CRC handbook of chemistry and physics, online: http://www.hbcpnetbase.com/.
[37]A. Ruzsinszky, J. P. Perdew, G. I. Csonka, O. A. Vydrov, and G. E. Scuseria, J. Chem. Phys. **126**, 104102 (2007).
[38]A. Ruzsinszky, J. P. Perdew, G. I. Csonka, O. A. Vydrov, and G. E. Scuseria, J. Chem. Phys. **125**, 194112 (2006).
[39]P. Mori-Sánchez, A. J. Cohen, and W. Yang, J. Chem. Phys. **125**, 201102 (2006).
[40]J. P. Perdew, R. G. Parr, M. Levy, and J. L. J. Balduz, Phys. Rev. Lett. **49**, 1691 (1982).
[41]Y. Zhang and W. Yang, J. Chem. Phys. **109**, 2604 (1998).
[42]L. K. Wagner, M. Bajdich, and L. Mitas, J. Comput. Phys. **228**, 3390 (2009).
[43]J. Kolorenč and L. Mitas, Rep. Prog. Phys. **74**, 026502 (2011).
[44]J. Kolorenč and L. Mitas, Phys. Rev. Lett. **101**, 185502 (2008).
[45]J. Kolorenč, S. Hu, and L. Mitas, Phys. Rev. B **82**, 115108 (2010).
[46]S. B. Zhang and J. E. Northrup, Phys. Rev. Lett. **64**, 2339 (1990).
[47]N. D. M. Hine, K. Frensch, W. M. C. Foulkes, and M. W. Finnis, Phys. Rev. B **79**, 024112 (2009).